Nuclear Materials and Energy 32 (2022) 101213

Contents lists available at ScienceDirect

Nuclear Materials and Energy

journal homepage: www.elsevier.com/locate/nme

Microstructural study of the thermal stability of a thermomechanically treated T91 steel by TEM in situ annealing

Elvira Oñorbe *, Mercedes Hernández-Mayoral, Rebeca Hernández, Marta Serrano

Division of Energy Interest Materials/CIEMAT. Madrid, Spain

ARTICLE INFO

Keywords:
Thermal stability
In situ experiments
Transmission electron microscopy

ABSTRACT

Thermal stability of a conventional 9Cr-1Mo ferritic/martensitic steel submitted to a thermomechanical treatment has been investigated by means of an in-situ annealing experiment up to 700 °C. For comparison, same experiment was carried out in the as received material, before thermomechanical treatment. The results showed an evolution of the microstructure in both cases, more acute for as received material. Before thermomechanical treatment, during annealing small precipitates within grain grew significantly, new ones precipitated and dislocations started to move around 600 °C, finding no effective obstacles to their movement and disappearing at grain boundaries and the free surface. After thermomechanical treatment, the microstructure developed was much more stable. Only a slight increase in the original precipitates size was observed and the dislocation structure remained stable after annealing. To compare the results of in-situ experiments, short term heat treatments up to 700 °C were carried out for both materials on bulk pieces. The principal difference observed was the dislocation density in the case of as received material. After in-situ experiment, the analyzed area was free of dislocations while after heat treatment a certain density of dislocations remained within grains. This fact can be related to the proximity of the free surface in the case of thin foils.

1. Introduction

Ferritic/martensitic (F/M) steels are candidates for structural materials in nuclear technologies thanks to their radiation and void swelling resistance, good thermal properties and good corrosion resistance [1,2]. However, in the study of mechanical properties, it has been found that the creep strength at high temperature, above 650 °C, is not good enough for critical components of power plants [3,4]. This loss of mechanical properties at high temperature has been attributed to a coarsening of the microstructure, a decrease of dislocation density and the coalescence of precipitates [5]. Therefore, the efforts have been focused on seeking solutions: development of new materials or the improvement of F/M steels.

One of the pathways to obtain materials able to work at higher temperatures has been the insertion of a fine dispersion of hard nano-oxide particles in the steel matrix stables at high temperature. In these oxide dispersion strengthened (ODS) alloys, the presence of nano-oxide particles enhances mechanical properties at high temperature as they act as effective barriers to dislocation motion, holding deformation and limiting grain growth. However, all the steps in the fabrication routes of ODS materials (gas atomization, mechanical alloying, consolidation and the final thermomechanical treatment) are complex and expensive and alternative materials and fabrication routes are being explored [6–9].

As for the improvement of F/M steels, tailoring the alloy chemistry or thermomechanical treatments have been employed to refine and stabilize their microstructure at high temperature service conditions, using similar criteria as for ODS alloys[5,10–14]. The family of 9–12 %Cr martensitic steels has a complex microstructure hardened by the presence of different precipitates: $M_{23}C_6$ carbides placed at prior austenite grain boundaries (PAGBs) and sub-grain boundaries together with MX carbides/nitrides at the interior of the grains and on sub-grain boundaries. Thermomechanical treatments allow obtaining a high dislocation density, entailing the presence of a higher number of nucleation sites for these precipitates. Therefore, a fine dispersion of stable precipitates within grains, as in the case of ODS alloys, will be obtained, acting as barriers to dislocation motion and pinning sub-grain boundaries, thus improving creep resistance of the material by the stabilization of the martensite transformation and the hardening role [10,15,16].

The next step has been the study of the thermal stability of this enhanced microstructure at operation temperatures. The microstructure

* Corresponding author.
E-mail address: elvionorbe@gmail.com (E. Oñorbe).

https://doi.org/10.1016/j.nme.2022.101213
Received 21 January 2022; Received in revised form 20 May 2022; Accepted 13 June 2022
Available online 26 June 2022

of 9Cr F/M steels with a thermomechanical treatment has been explored by some authors before and after creep exposure showing a resistance to coarsening of Cr rich carbides in the thermomechanically treated condition [15]. In the case of MX precipitates, they were found to be still present even after prolonged exposures at 650 °C and, for 9Cr steels the undesirable transformation of MX to Z-phase (thermodynamically more stable) is retarded compared with higher Cr steels, since its formation is a strong function of the available Cr. This transformation has an important influence in the long-term creep strength of the material and premature breakdown of creep strength has been associated to the presence of Z-phase in 11–12 wt% Cr steels, while MX precipitates are stable even after long term exposures at 650 °C in 9 %Cr steels [17,18]. Sawada et al. [19] in 2001, observed that in a 9Cr steel MX precipitates grew after long-term creep experiments and the size distribution curve became broader with increasing aging time. Last works concerning creep behavior where the stability of precipitates was studied somehow, suggests a relatively low coarsening rate for MX precipitates [20,21]. Concerning thermomechanically treated 9Cr steels no references about the size evolution of MX precipitates or their dynamic behavior have been found.

In this work, a thermomechanical treatment, described in [22] and following previous investigations [23], was used on conventional 9Cr-1Mo ferritic/martensitic steel, with the purpose of increasing the dislocation density and thereby obtaining a homogeneous distribution of fine precipitates within grains. The study of the mechanical properties by means of creep tests at high temperature, revealed an improvement of the thermomechanically treated compared to the as received material [22–24], that was attributed to the fine dispersion of MX carbides/nitrides and $M_{23}C_6$ observed in the analysis of the initial microstructure, before creep tests in the case of the thermomechanically treated alloy, by Scanning Electron Microscopy (SEM) and Transmission Electron Microscopy (TEM) reported in previous works [22,23]. But, it would be necessary to know whether in fact these precipitates are stable and how they evolve with temperature and therefore the role they play in maintaining good behavior at high temperature.

The objective of the present work is to assess the thermal stability of the microstructural features with temperature. With this propose in situ TEM annealing experiments up to 700 °C were carried out in the thermomechanically treated T91 steel as well as in the as-received T91 steel for comparison. With these experiments it is possible the direct observation of the evolution of the microstructural features, precipitates and dislocations, with temperature. In addition, the effect of using thin foils for in situ TEM experiments was also intended to be ascertained. This was done by performing ex-situ annealing treatments in both materials up to the same temperature reached at the in situ annealing experiments, 700 °C. Afterwards their microstructure was studied also by TEM allowing differentiation between those changes related with the heat treatment and those related with the sample thickness.

2. Materials and methods

The studied material was a hot rolled plate of commercial T91 steel, from now on AR, provided by INDUSTEEL (ArcelorMittal), Belgium. The chemical composition of the commercial T91 is given in Table 1.

With the goal of improving mechanical properties by modifying the microstructure, a plate of 40x123x295 mm was thermomechanically treated by COMTES FHT, Czech Republic. From now on this material will be referred as TMT. The fabrication route of TMT material is well described in [22], in brief, austenitizing treatment at 1227 °C for 30 min followed by ausforming at 900 °C with a 20% reduction by rolling. The material was air cooled, afterwards tempered at 740 °C for 130 min and finally, air cooled.

Table 1
Chemical composition of commercial T91 (wt. %).

	Cr	Mo	Mn	Si	V	C	Nb	N	Fe
T91	9.0	1.0	0.4	0.4	0.2	0.1	0.07	0.03	Bal.

The study of the thermal stability of the microstructure was addressed by in situ annealing experiments inside a TEM JEOL JEM-2010 with LaB_6 filament and operating at 200 keV available at CIEMAT facilities. The samples studied were 3 mm diameter discs, 0.1 mm thick, with a final electrolytic polishing with a mixture of 5% perchloric acid and methanol, at −60 °C. The Gatan 652 model double tilt heating holder employed is a tantalum furnace type holder designed to allow direct observation of microstructural changes during the experiment. Temperature ramp for each material, AR and TMT, was designed according to mechanical properties and microstructural results obtained in a previous work [22], where the creep behavior of AR and TMT materials were studied by short term rupture tests at 600 °C, 650 °C and 700 °C..In the case of the AR, the temperature was raised at a rate of 20 °C/min, stopping every 100 °C to observe the behavior of the material and reorient the sample to keep the correct imaging conditions throughout the experiment. Once 600 °C were reached, the temperature was kept for 30 min and, after this period and the adjustment of the orientation conditions, heated up again at 20 °C/min up to 700 °C. This second isotherm was also kept for 30 min. The total duration of the experiment was about 3 h including cooling time. In the case of TMT, an intermediate additional isotherm at 650 °C for 15 min was included, being the total experiment time similar to AR.

A video was recorded throughout the course of the experiments at a rate of 30 fps employing Bright Field conditions where defects and precipitates were visible. Still shots were also taken at 600 °C, 700 °C in the case of AR and at 500 °C, 600 °C, 650 °C and 700 °C in the case of TMT. At each temperature the selected region was properly oriented to observe the evolution of some selected features.

With the aim to study the thermal stability of the microstructure and compare with the one developed after in situ annealing, small bulk pieces of both materials were subjected to a heat treatment at 700 °C in a tubular furnace under Argon atmosphere for 6 h and cooled inside the furnace up to room temperature. The differences in the resultant microstructure between thin foils and bulk materials were analysed.

Table 2 gives a summary of the studied materials and the corresponding material code.

The microstructure of the different material conditions studied in this work were analysed, in the case of AR, TMT, AR-HT and TMT-HT, by Scanning Electron Microscopy/Electron BackScattered Diffraction (SEM/EBSD) using Channel 5 EBSD software on a Hitachi SU6600 field emission gun scanning electron microscope (FEG-SEM) equipped with an Oxford Instruments HKL Nordlys detector. TEM was also employed in the microstructural study of all the conditions shown in Table 2 using standard imaging methods of Bright Field (BF) in a TEM JEOL JEM-2010 with LaB_6 filament operating at 200 keV available at CIEMAT. The analysed samples were 3 mm diameter discs prepared as has been described previously.

Size distribution and number density of the different families of precipitates found in the alloy were measured using SEM and TEM images employing JMicroVision software [25]. For the analysis, more than 2500 precipitates for SEM and more than 500 precipitates for TEM were measured in at least 10 images of different regions. Number density was

Table 2
Material Code and description of the corresponding condition.

Material Code	Description
AR	Commercial, as received, T91 alloy
TMT	Thermomechanically treated T91 alloy
AR-ISA	T91 in situ annealed up to 700 °C
TMT-ISA	T91 thermomechanically treated and in situ annealed up to 700 °C
AR-HT	T91 heat treated at 700 °C during 6 h
TMT-HT	T91 thermomechanically treated and heat treated at 700 °C during 6 h

obtained by counting precipitates in the same images where the size was measured, and divided by the analysed area (SEM) or volume (TEM). Dislocation density was estimate by direct measurements of their length in representative TEM images and divided by the analysed volume. TEM thickness measurements were done employing Convergent Beam Electron Diffraction (CBED) method [26]. Finally, Energy Dispersive Spectroscopy (EDS) for TEM was used to obtain the composition of the precipitates present in the alloy.

3 Results.

1.2. Initial microstructure

Initial microstructure of the AR and TMT materials is widely described in [22]. AR consists in tempered martensite with a prior austenite grains (PAGs) of (20 ± 2) μm and lath width of (275 ± 19) nm, with Cr rich carbides, with a mean size value of (135 ± 2) nm and a number density of (3.4 ± 0.2) × 10^{12} m^{-2}, decorating PAGs, packets, blocks and lath boundaries that have been formed during tempering. Few isolated MX precipitates were also detected by TEM within grains and the dislocation distribution was inhomogeneous and changed from one grain to another. The dislocation density estimated was about (4.5 ± 0.4) × 10^{14} m^{-2}. In the case of TMT material, there was a large increase of the PAG size in the range of 150–170 μm, but not significant differences were found in the lath width, (270 ± 18) nm, nor in the Cr rich carbides size distribution, mean size (127 ± 2) nm and the same number density as AR material, (3.4 ± 0.2) × 10^{12} m^{-2}. After the thermomechanical treatment, a fine distribution of MX precipitates was observed within grains by means of TEM. Two types of MX precipitates were distinguished and are shown in Fig. 1 (a). The Electron Dispersive Spectroscopy (EDS) analysis (Fig. 1 (b)) indicated that the ones with an ellipsoidal morphology were Nb rich carbides (black arrows in Fig. 1 (a)) and the ones with needle shape morphology were identified as V(C, N) (white arrows in Fig. 1 (a)). The mean size and density were (6.5 ± 0.3) nm and (4.5 ± 0.6) × 10^{21} m^{-3} respectively. A high dislocation density was observed but the distribution was inhomogeneous, changing from one grain to another. In the case of TMT steel, dislocations were pinned at MX precipitates. The dislocation density estimated was in the same range than AR material, about (4.5 ± 0.3) × 10^{14} m^{-2}.

1.3. In situ annealing TEM experiments

Fig. 2 corresponds to bright field still shots taken at the initial state, at 600 °C and at 700 °C. Previous to the starting of the experiment, a representative area of the material was selected and properly oriented to follow the evolution of the different features during the experiment. It is worth noting that both, at the starting of the experiment as well as all along the experiment, the imaging conditions were carefully selected in order to obtain the better contrast and visibility of the microstructural features (B = [1 1 1], g=(0 1 1)). Fig. 2 (a) shows the selected region, very close to a grain boundary, where a few precipitates and pinned dislocations can be distinguished. One dislocation and a possible precipitate have been indicated as references in the image of the initial microstructure (black dotted line and white circle respectively) and also in the images of this region at the different temperatures reached during the experiment.

At the beginning of the experiment, during the initial temperature ramp, no noticeable changes were observed up to 600 °C and the microstructure remained the same. It is at the beginning of the 600 °C isotherm (Fig. 2 (b)) when pre-existing MX precipitates began growing rapidly (e.g. the one inside the white circle and features in the vicinities of the reference dislocation) compared with the initial state (Fig. 2 (a)). Qualitatively, during the isotherm most of preexisting precipitates have increased their size. Regarding dislocation evolution, a few movements were observed at this point of the experiment, but most of dislocations remained pinned at their original position.

Fig. 2 (c) was taken just after reaching 700 °C. Observing the same references (black dotted line and white circle), MX precipitates continued growing and new ones precipitated within grains. From this point on, the microstructure evolved very fast. By the end of the experiment the matrix was almost free of dislocations and an oxide layer has been formed.

Fig. 3 shows a sequence of frames extracted from the recorded video after 20 min at the isotherm at 700 °C where a dislocation moves form the initial pinning point to the grain boundary. Dislocations were activated around 600 °C and their movement continued until the end of the experiment.

For TMT material, as in the case of AR, still shots were taken at different temperatures during the experiment. The initial microstructure and the sequence of still shots are shown in Fig. 4. The sample was

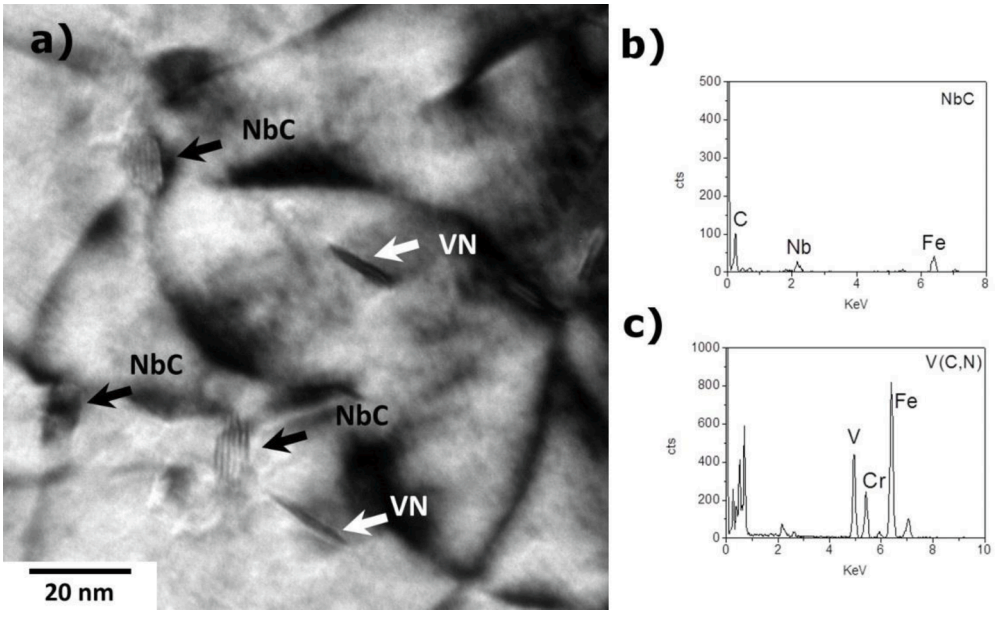

Fig. 1. a) Bright field TEM image of TMT showing the presence of small precipitates, b) EDS results of a Nb rich carbide (black arrows) and V(C,N) precipitates (white arrows).

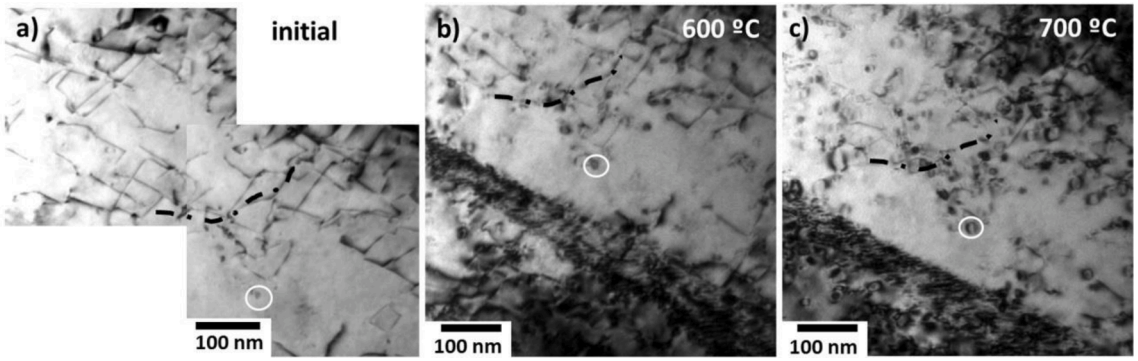

Fig. 2. Bright field images taken during the in situ annealing experiment, AR material. a) Initial state, b) at the beginning 600 °C and c) after reaching 700 °C.

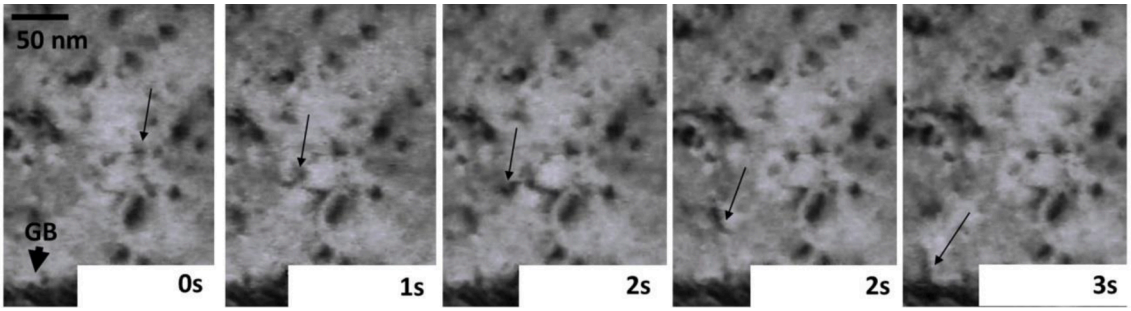

Fig. 3. Sequence of frames extracted from the recorded video showing the movement of a dislocation towards a grain boundary. The images correspond to the isotherm after 20 min at 700 °C.

oriented properly to have a good contrast of the different features (Fig. 4 (a)) and two references were chosen to keep the same area during the experiment, a precipitate (black circle) and a dislocation (dashed black line). As in the case of AR material, the first changes seem to take place around 600 °C (Fig. 4(b)). At this temperature the coarsening of pre-existing MX precipitates was clearly observed, and some dislocations started to move from their initial position. From this point on, the microstructure had scarcely progressed. No important coarsening of precipitates was observed neither at 650 °C nor at 700 °C (Fig. 4 (c) and (d) respectively) and dislocation movements were jerky and not very frequent. An example of a sequence of frames extracted from the video after 20 min at 700 °C is shown in Fig. 5. The dislocation moves from their initial position finding a first obstacle, an MX precipitate, where it remains pinned for 2 s and then moves to the next obstacle where remains pinned for another 2 s.

Finally, the evolution on the precipitate size has been quantified in the charts shown in Fig. 6. Coarsening of precipitates started at 600 °C and in the case of AR material, continued during the isotherm at 700 °C even doubling the initial size (Fig. 6 (a)). In the case of TMT material the maximum size was reached during the isotherm at 600 °C and after this period, particle size remained stable (Fig. 6(b)).

1.2. Ex situ heat treatment

Fig. 7 (a) shows the microstructure of the AR material resulting from ex situ heat treatment at 700 °C, for 6 h, from now on, AR-HT, which consists in tempered martensite. PAGs have a mean size of (20 ± 1) μm. and Cr rich carbides are decorating PAGs, packet, block and lath boundaries (Fig. 7 (b)). The size distribution is represent in Fig. 7 (c) being the mean size value (152 ± 2) nm and the number density (2.7 ± 0.2) × 10^{12} m^{-2}. The Inverse Pole Figure (IPF) map corresponding to the AR-HT is shown in Fig. 7 (d). A random grain orientation can be observed.

Fig. 7 (e), (f) and (g) show bright field TEM images of AR-HT material. Lath width has been estimated using TEM images as the one shown in Fig. 7 (e), being the mean value (250 ± 15) nm. Also, from TEM analysis, dislocation number density was measured being (2.4 ± 0.3) × 10^{14} m^{-2}. Cr rich carbides were identified by EDS analysis (white arrows in Fig. 7 (e)) and small MX precipitates were observed placed at the interior of the grains, isolated or in small groups (black arrows and black circles respectively in Fig. 7 (f)). High magnification images, like the one shown in Fig. 7 (g) with a detail of MX precipitates were used to estimate the mean size, being (12 ± 2) nm.

Fig. 8 (a) shows the microstructure of the TMT-HT. PAGs have a mean size of 170 μm and Cr rich carbides are placed at PAGBs, packet, block and lath boundaries (Fig. 8 (b)). The size distribution is represented in Fig. 8 (c) with a mean size of (130 ± 2) nm and a number density of (2.4 ± 0.2) × 10^{12} m^{-2}.

The IPF map corresponding to the TMT-HT is shown in Fig. 8 (d). Inside PAGs, different laths orientations can be distinguished.

In the case of TMT-HT, Fig. 8 (e) shows Cr rich carbides mainly placed at grain boundaries (black arrows) and a fine distribution of MX precipitates within grains (white arrows). Lath width has been estimated being the mean value (264 ± 12) nm. In Fig. 8 (f), dislocations appear pinned at MX precipitates with a number density of (3.7 ± 0.3) × 10^{14} m^{-2}. In the case of TMT-HT the MX mean size measured was (10.2 ± 0.3) nm and the density corresponds to (5.2 ± 0.3) × 10^{21} m^{-3}.

Finally, Table 3 lists the quantitative results obtained for all the conditions studied.

4. Discussion

In this work, in situ TEM annealing experiments have been employed to analyze the thermal stability of the microstructure of a thermo-mechanically treated 9Cr-1Mo ferritic/martensitic steel (TMT). Those results have been compared with an in situ annealing experiment carried out on the same material in the as received condition (AR). The effectiveness of this experimental technique has been tested as a reliable tool

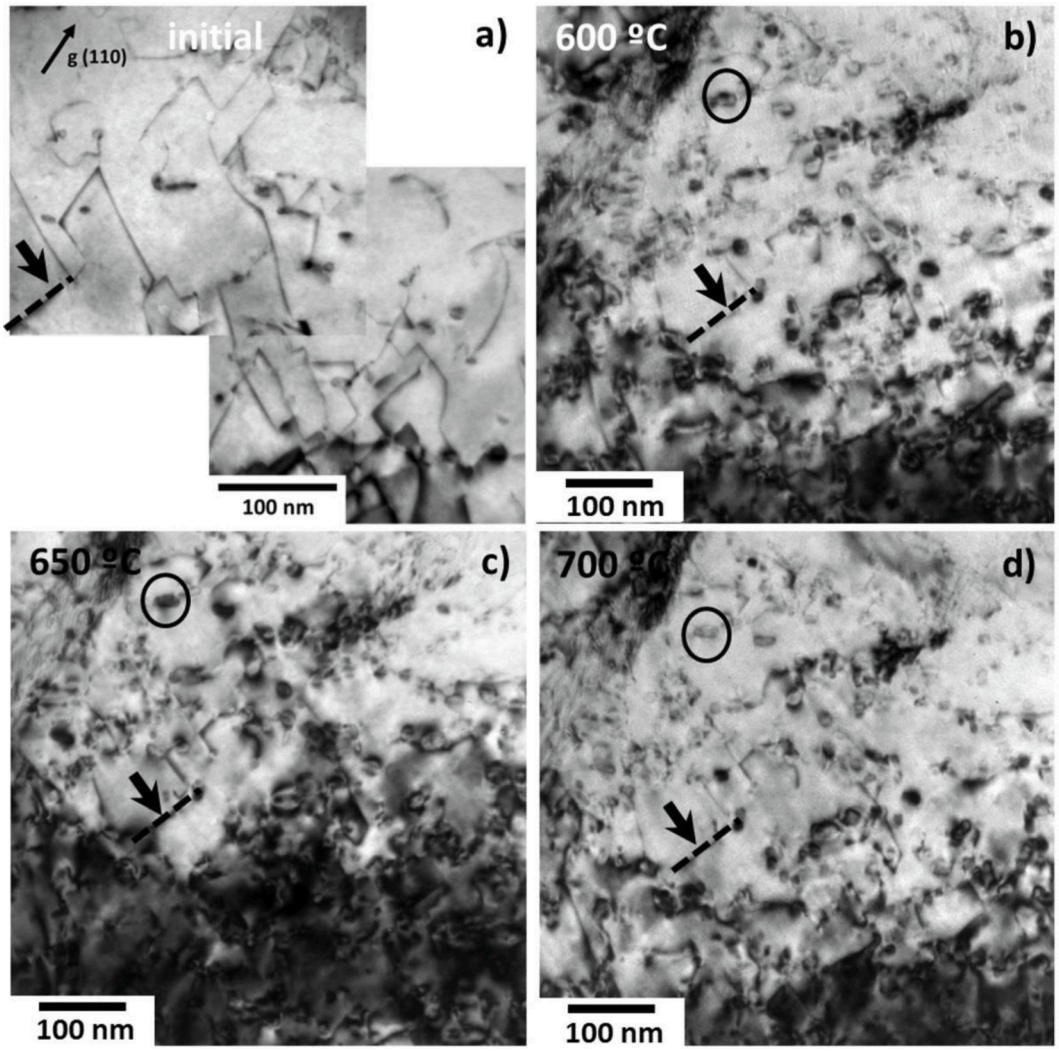

Fig. 4. Bright field images of TMT taken during the annealing in situ experiment. a) At the initial stage, b) at 600 °C, c) at 650 °C and d) at 700 °C.

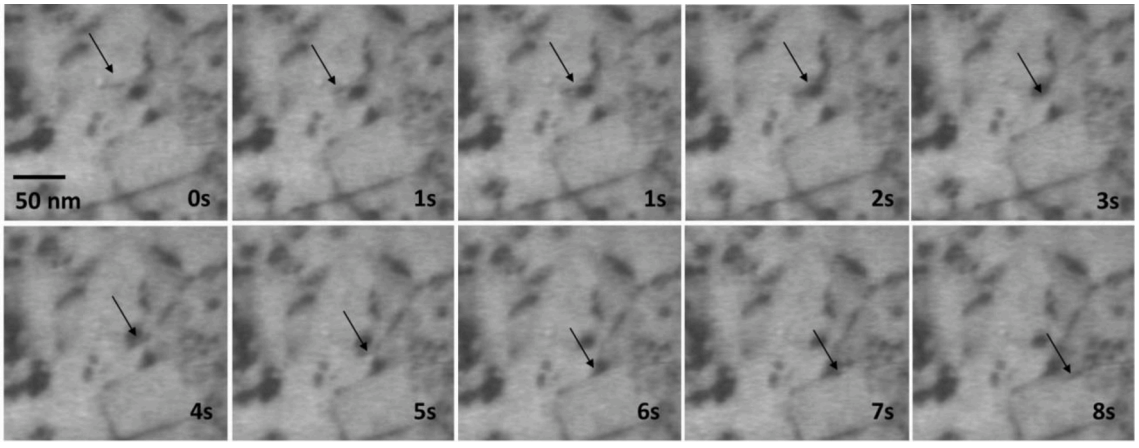

Fig. 5. Sequence of frames extracted from the recorded video, TMT material, showing the movement of a dislocation. The images correspond to the isotherm after 20 min at 700 °C.

to study the dynamic evolution of the microstructure, comparing the microstructure at the end of the experiment of both materials with the one developed after ex situ short-term heat treatments to verify the results obtained by in situ experiments.

In general, an evolution of the microstructure has been observed in the AR and TMT materials during in situ annealing but also after short-term thermal treatment at 700 °C. In the case of in situ annealing experiments this evolution starts around 600 °C and it is substantially

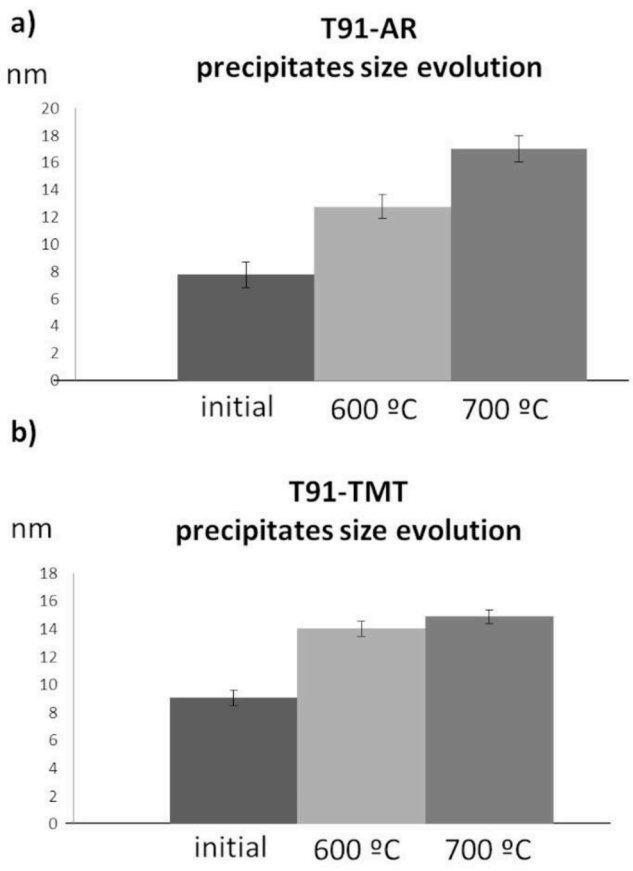

Fig. 6. Precipitate size evolution charts during in-situ annealing experiments for a) AR and b) TMT materials.

more acute for AR material, meaning that, as expected, thermomechanical treatment stabilizes the microstructure at high temperature. The first microstructural changes observed as temperature increases were those related with the evolution of the different families of precipitates present in the alloys. The coarsening of MX precipitates in the TMT material is negligible and only a slight increase in the mean size around 650 °C has been observed. On the contrary, new precipitates and a considerable coarsening of MX precipitates occurred during in situ annealing in the case of AR material. These results were verified by short-term heat treatments in both materials. For TMT material the change in the mean size of MX precipitates was from (6.5 ± 0.3) nm to (10.2 ± 0.3) nm after 6 h at 700 °C with a little further evolution in their density (Table 3). In the case of AR material, before annealing only isolated MX precipitates were found and after heat treatment new precipitates were distributed either isolated or forming small groups with a mean size of (12 ± 2) nm. In general, according to literature, it has been considered that MX precipitates are stable and no significant coarsening occurs during ageing or creep [10,19,27–30]. However there are also works where MX coarsening is evident above 650 °C [31,32]. MX coarsening in these materials could be enhanced by the diffusion along dislocations and lath and sub-grain boundaries. As has been described before, these materials have a high dislocation density and therefore, the pipe diffusion becomes important and may contribute to the coarsening of precipitates as well as lattice diffusion [32].

The other family of precipitates studied in this work was Cr rich carbides. Only a coarsening of a 13% was observed for Cr rich precipitates in the case of AR material after short term heat treatment. The differences in the evolution of the mean size of Cr rich precipitates observed in the case of TMT are within the margin of error and therefore we can consider that are stable. The coarsening of Cr rich carbides has been previously reported and starts at temperatures above around 550 °C [33]. The coarsening in the case of AR material may well be because has a higher density of PAGBs where the degree of disorder is higher than in lath boundaries [30]. Thus, the coarsening rate of Cr rich carbides is greater in the vicinity of PAGBs than within grains due to the enhanced diffusion processes.

The evolution of dislocations during annealing was also analyzed in both materials. In the as received condition no differences have been observed between the two materials, AR and TMT: similar density and an inhomogeneous distribution of dislocations, changing from grain to grain. During in situ annealing experiments the extinction of dislocations is much more accused in the case of AR-ISA than in the case of TMT-ISA. Dislocations can move easily in the former at high temperatures, since there are no obstacles, particles or other dislocations, or not strong enough and they can move to grain boundaries or the sample surface to disappear. The activation of the movement of dislocations with temperature starts at 600 °C and does not end until the end of the experiment, where the material seems to be free of dislocations. By contrast, in the case of TMT-ISA material, dislocations were pinned at different points, generally the small precipitates, that are strong enough to retain dislocations, preventing them to reach boundaries and be absorbed, until the end of the experiment. Therefore, even though in TMT-ISA there was a small increase in the mean size value of MX precipitates, as has been explained before, that may result in a loss of strengthening, on the contrary, a high dislocation density still remains within the matrix at the end of the in situ experiment. Regarding the evolution of dislocations after short term heat treatment, there is a decrease in the dislocation density in both materials compared to the initial state (Table 3). In the case of the TMT material this decrease is lower, as expected, due to the presence of a fine distribution of MX precipitates that retain dislocations. The most striking difference was found between the resulting dislocation distribution and density of AR-HT and the one after in situ experiments, AR-ISA, where grains where almost free of dislocations at the end of the experiment. This difference can be explained in the fact that in situ experiment are carried out with thin films of around 100 nm that placed dislocations near the free surface, that may act as a sink for dislocations, and therefore, are able to escape [33] and at the end of the experiment grains are almost free of dislocations in contrast with the density of $(2.4 \pm 0.3) \times 10^{14} m^{-2}$ estimated for AR-HT.

Another microstructural change that must be considered is the evolution of sub-grain boundaries, since part of the improvement of the creep resistance at high temperatures can be associated to a direct effect of the sub-boundary hardening. Due to the differences observed in the MX size and distribution in both materials, it would be expected to find differences also in the lath width as a result of such evolution. Indeed, some authors have observed a decrease in the lath width related to the presence of defects and precipitates generated during the thermomechanical treatment, that impede the growth of the martensite laths [15,34,35]. In our case, no differences in the lath width have been observed from AR material to TMT material that can be associated with the thermomechanical process followed to obtain the fine distribution of precipitates, nor after heat treatment. This can be explained because lath width is directly related with the tempering temperature and the time of duration, being larger for higher temperatures and longer term treatments [36,37]. In this work, the tempering was done at 740 °C during relatively long time, 130 min, which implies that there is an increase of martensitic laths after thermomechanical process without a refinement of the lath width compared with AR material and also a recovery of the dislocation tangles formed, finding a similar dislocation density in both materials.

Finally, the possible effects of particular experimental conditions of in situ experiments, as can be the electron beam or the use of thin foils have been also evaluated according to the results of in situ and ex situ experiments. The observed evolution of the microstructure, either directly at the in situ experiments of a thin foil with no more than a hundred nanometers thickness in the region studied by TEM, or after

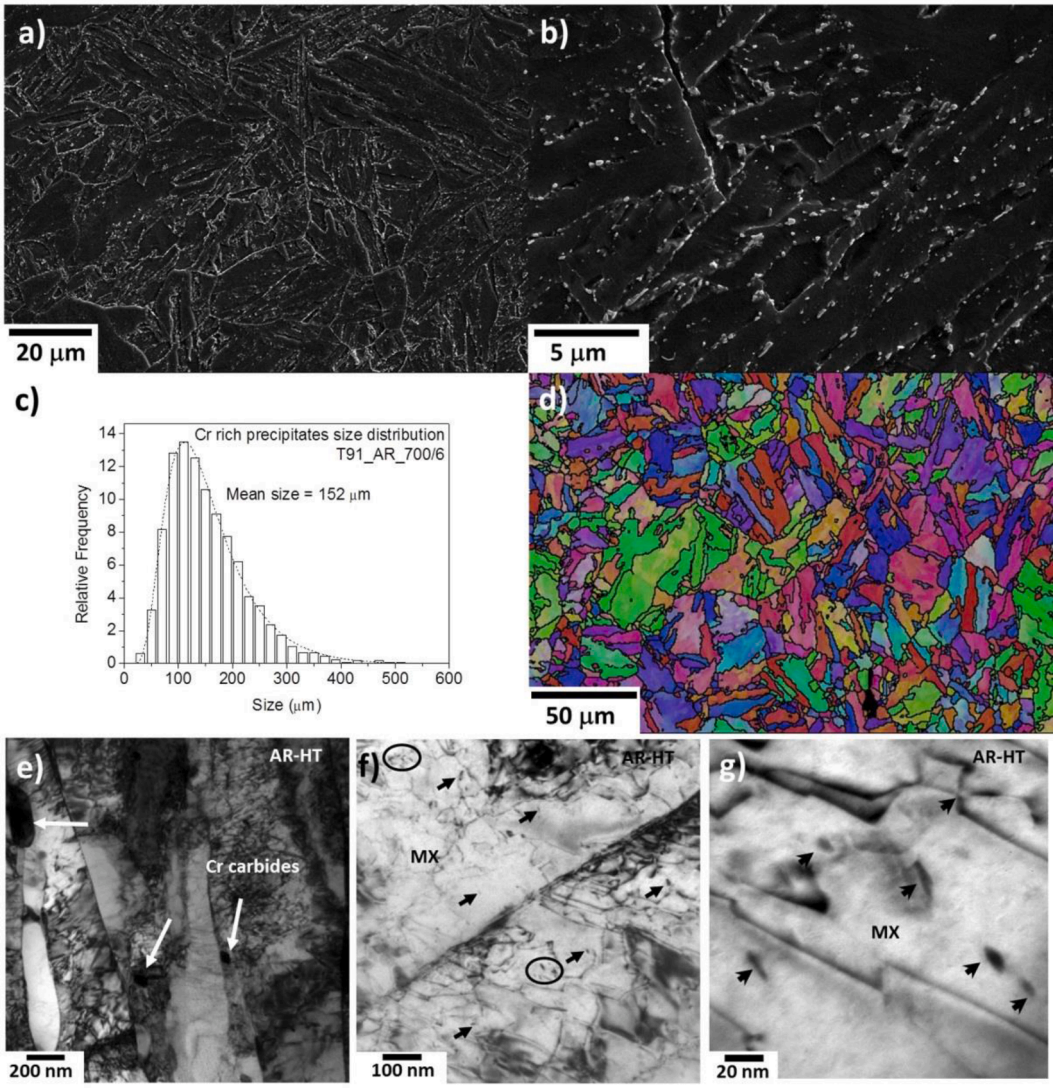

Fig. 7. a) Secondary electron image of the microstructure of AR-HT where PAGBs are distinguished, b) secondary electron image of the microstructure of **AR-HT** where the distribution of Cr rich carbides can be observed, c) Cr rich carbides size distribution, d) IPF map e) bright field TEM image with the laths and Cr rich carbides f) a lath boundary and MX precipitates within grains with an inhomogeneous distribution (black arrows and circles) and g) MX precipitates distribution and pinned dislocations.

heat treatment of a bulky specimen, has been shown to follow similar trends and both types of investigation are well complementary. It is well known that the properties of materials can be different between nanometer size and bulk material. The only evident difference observed between both experiments was the dislocation density in the case of AR material. After heat treatment the dislocation density was $(2.4 \pm 0.3) \times 10^{14}$ m^{-3} but at the end of the in situ annealing experiment the sample was almost free of dislocations. Synergetic effects can be related to this result. On one side, in the microstructure of AR material, as has been described above, there are no obstacles or strong enough to dislocation movements. On the other side, there are those causes related with the experimental conditions: the beam energy that can promote the activation of dislocation movements and also the proximity of the sample surface that may act as a predominant sink for dislocations. The activation of dislocation movements due to beam effects has been observed in the case of aluminum and gold films during in situ TEM deformation experiments [38], but it is not expected in the case of Fe with a beam energy of 200 keV.

5. Conclusions

The thermal stability of a thermomechanical treated 9Cr-1Mo ferritic/martensitic steel has been evaluated by means of electron microscopy techniques. The main points that may be drawn are:

- Before thermomechanical treatment, during annealing MX precipitates within grains grew significantly, new ones precipitated and dislocations started to move around 600 °C, finding no effective obstacles to their movement and disappearing at grain boundaries and the free surface. After thermomechanical treatment, the microstructure developed was much more stable. Only a slightly increase in the original MX precipitates size was observed and the dislocation structure remained stable after annealing. The increase in the precipitate size can be associated with the contribution of pipe diffusion to their coarsening.
- The mean size of Cr rich carbides for AR material increases a 13%. This increase may be associated with a higher density of PAGBs where diffusion processes are enhanced.
- Initially the density and distribution of dislocations were similar for AR and TMT materials but in the case of AR material the density

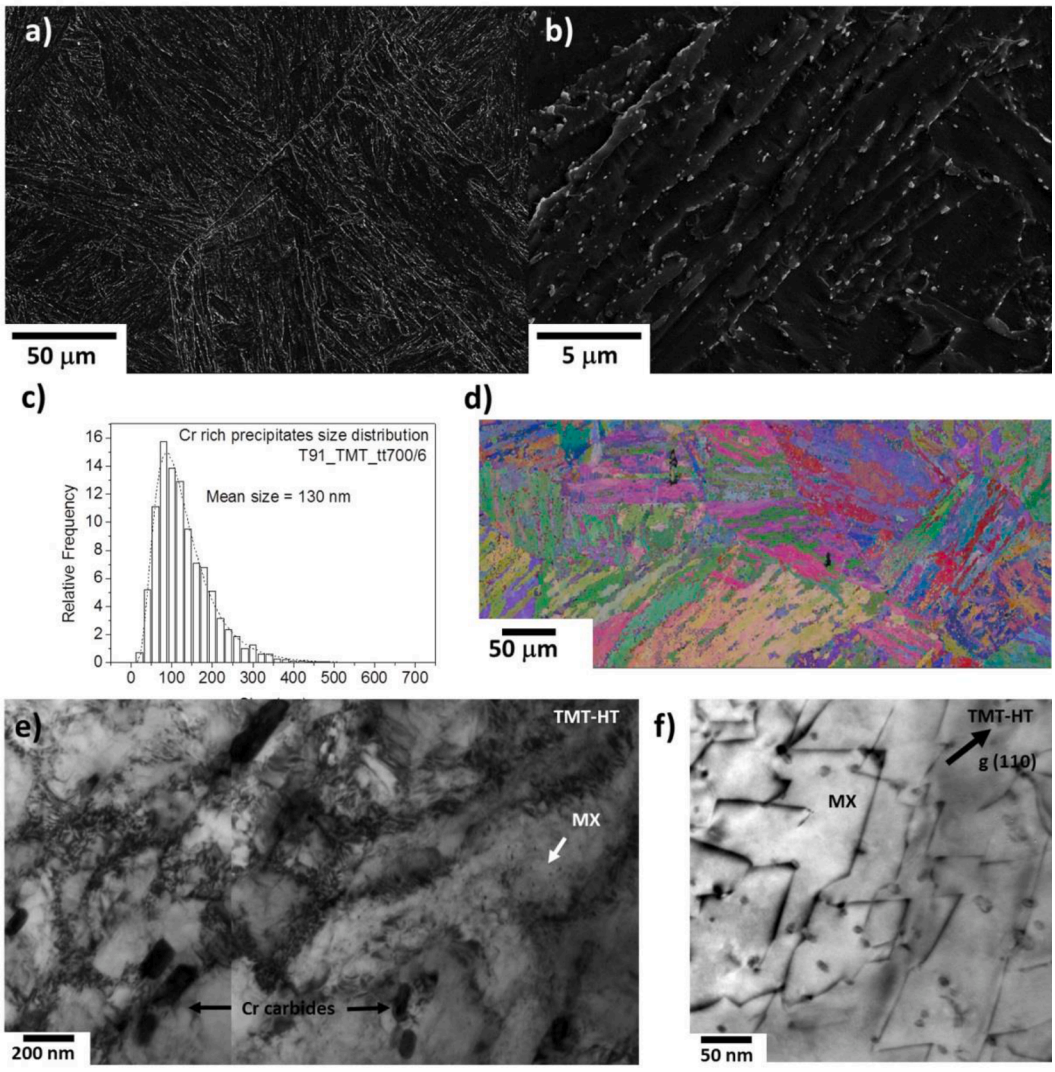

Fig. 8. a) Secondary electron image of the microstructure of TMT-HT where PAGBs are distinguished, b) secondary electron image of the microstructure of TMT-HT where the distribution of Cr rich carbides can be observed, c) Cr rich carbides size distribution, d) IPF map e) and f) Bright field TEM images of Cr rich carbides and MX precipitates distribution (black and white arrows respectively) and a detail of the MX distribution and their interaction with dislocations.

Table 3
Summary of the results.

	CrC (nm)	ρ(CrC) (10^{12} m^{-2})	ρ (dislocation) (10^{14} m^{-2})	Lath width (nm)	MX (nm)	ρ (MX) (10^{21} m^{-3})
AR	135 ± 2	3.4 ± 0.2	4.5 ± 0.4	275 ± 19	**	**
TMT	127 ± 2	3.4 ± 0.2	4.5 ± 0.3	270 ± 18	6.5 ± 0.3	4.5 ± 0.6
AR-HT	152 ± 2	2.7 ± 0.2	2.4 ± 0.3	250 ± 15	12 ± 2	**
TMT-HT	130 ± 2	2.4 ± 0.2	3.7 ± 0.3	264 ± 12	10.2 ± 0.3	5.2 ± 0.3

**Not measured.

decreased after short-term heat treatment and drastically after in situ experiments. In the case of AR material dislocations can move easily at high temperatures, since there are no obstacles, or not strong enough and they can reach grain boundaries or the free surface, in the case of thin foils, to disappear.

Data availability

The raw/processed data required to reproduce these findings cannot be shared at this time as the data also form part of an ongoing study.

CRediT authorship contribution statement

Elvira Oñorbe: Conceptualization, Methodology, Formal analysis, Investigation, Writing – original draft. **Mercedes Hernández-Mayoral:** Conceptualization, Methodology, Supervision. **Rebeca Hernández:** Conceptualization, Resources. **Marta Serrano:** Conceptualization, Resources.

Declaration of Competing Interest

The authors declare that they have no known competing financial interests or personal relationships that could have appeared to influence the work reported in this paper.

Acknowledgements

This work is supported by the National project FERRONESS

(Mat2016-80875). The authors want to acknowledge also to Mr. M. González-Castaño for TEM sample preparation and his support with in situ TEM experiments.

References

[1] R.L. Klueh, A.T. Nelson, Ferritic/martensitic steels for next generation reactors, J. Nucl. Mat. 371 (2007) 37–52, https://doi.org/10.1016/j.jnucmat.2007.05.005.

[2] F. Abe, Research and Development of Heat-Resistant Materials for Advanced USC Power Plants with Steam Temperatures of 700 °C and Above, Engineering 1 (2) (2015) 211–224, https://doi.org/10.15302/J-ENG-2015031.

[3] P. Dubuisson, Y. de Carlan, V. Garat, M. Blat, ODS Ferritic/martensitic alloys for Sodium Fast Reactor fuel pin cladding, J. Nucl. Mater. 428 (2012) 6–12, https://doi.org/10.1016/j.jnucmat.2011.10.037.

[4] J.S. Cheon, C.B. Lee, B.O. Lee, J.P. Raison, T. Mizuno, F. Delage, J. Carmack, Sodium fast reactor evaluation: Core materials, J. Nucl. Mater. 392 (2009) 324–330, https://doi.org/10.1016/j.jnucmat.2009.03.021.

[5] S. Hollner, B. Fournier, J. Le Pendu, T. Cozzika, I. Tournié, J.-C. Brachet, A. Pineau, High-temperature mechanical properties improvement on modified 9Cr-1Mo martensitic steel through thermomechanical treatments, J. Nucl. Mater. 405 (2010) 101–108, https://doi.org/10.1016/j.jnucmat.2010.07.034.

[6] F. Bergner, I. Hilger, J. Virta, J. Lagerbom, G. gerbeth, S. Connolly, Z. Hong, P.S. Grant, T. Weissgärber, Alternative Fabrication Routes towards Oxide-Dispersion-Strengthened Steels and Model Alloys, Metall Mat Trans A: Phys Mettal. Mater. Sci. 47(11) (2016) 5313-5324. Doi: 10.1007/s11661-016-3616-2.

[7] I. Hilger, X. Boulnat, J. Hoffmann, C. Testani, F. Bergner, Y. de Carlan, F. Ferraro, A. Ulbricht, Fabrication and characterization of oxide dispersion strengthened (ODS) 14Cr steel consolidated by means of hot isostatic pressing hot extrusion and spark plasma sintering, J. Nucl. Mater. 472 (2016) 206–214, https://doi.org/10.1016/j.jnucmat2015.09.036.

[8] G.R. Odette, N.J. Cunningham, T. Stan, M.E. Alam, Y. de Carlan, Chapter 12: Nano-oxide dispersion strengthened steels, Structural Alloys for Nuclear Energy Applications, Elsevier, (2019) 529-583, Doi: 10.1016/B978-0-12-397046-6.00012-5.

[9] S. Ukai, S. Ohtsuka, T. Kaito, Y. de Carlan, J. Ribis, J. Malaplate, Chapter 10: Oxide dispersion strengthened/ferrite-martensite steels as core materials for Generation IV nuclear reactors, Struct. Mater. Generat. IV Nucl. React., (2017) 357-414, Doi: 10.1016/B978-0-08-100906-2.00010-0.

[10] F. Abe, Precipitate design for creep strengthening of 9%Cr tempered martensitic steel for ultra-supercritical power plants, Sci. Technol. Adv. Mater., 9 (2008) 013002, Doi: 10.1088/1468-6996/9/1/013002.

[11] S.S. Samant, I.V. Singh, R.N. Singh, Influence of intermediate rolling on mechanical behavior of modified 9Cr-1Mo steel, Mat. Sci. Eng. A 738 (2018) 135–152, https://doi.org/10.1016/j.msea.2018.09.092.

[12] L. Tan, D.T. Hoelzner, J.T. Busby, M.A. Sokolov, R.L. Klueh, Microstructure control for high strength 9Cr ferritic-martesitic steels, J. Nucl. Mat. 422 (2012) 45–50, https://doi.org/10.1016/j.jnucmat.2011.12.011.

[13] M. Song, C.Sun, Z. Fan, Y. Chen, R. Zhu, K.Y. Yu, K.T. Hartwig, H. Wang, X. Zhang., A roadmap for tailoring the strength and ductility of ferritic/martensitic T91 steel via thermo-mechanical treatment, Acta Mater., 112 (2016) 361-377, Doi: 10.1016/j.actamat.2016.04.031.

[14] D.T. Hoelzer, C.P. Massey, S.J. Zinkle, D.C. Crawford, K.A. Terrani, Modern nanostructured ferritic alloys: A compelling and viable choice for sodium fast reactors fuel cladding applications, J. Nucl. Mater. 529 (2020), 151928, https://doi.org/10.1016/j.jnucmat.2019.151928.

[15] P. Prakash, J. Vanaja, G.V. Prasad Reddy, K. Laha, G.V.S. Nageswara Rao, On the effect of thermo-mechanical treatment on creep deformation and rupture behavior of a reduced activation ferritic-martensitic steel, J. Nucl. Mater. 520 (2019) 65-77, Doi: 101016/jjnucmat201904014.

[16] R.L. Klueh, N. Hashimoto, P.J. Maziasz, Development of new nanoparticle strengthened martensitic steels, Scripta Mater 53 (2005) 275–280, https://doi.org/10.1016/j.scriptamat.2005.04.019.

[17] H.K. Danielsen, J. Hald, Behaviour of Z-phase in 9–12%Cr steels, Energy Mater. 1 (2006) 49–57, https://doi.org/10.1179/174892306X99732.

[18] M. Yoshizawa, M. Igarashi, K. Moriguchi, A. Iseda, H.G. Armaki, K. Maruyama, Effect of precipitates on long-term creep deformation properties of P92 and P122 type advanced ferritic steels for USC power plants, Mat. Sci. Eng. A 510-511 (2009) 162–168.

[19] K. Sawada, K. Kubo, F. Abe, Creep behavior and stability of MX precipitates at high temperature in 9Cr–0.5Mo–1.8W–VNb steel, Mater. Sci. Eng.: A 319-321 (2001) 784–787.

[20] Y. Zeng, J. Jia, W. Cai, S. Dong, Z. Wang, Effect of long-term service on precipitates in P92 steel, Int. J. Miner. Metall. Mater. 25 (2018) 913–921, https://doi.org/10.1007/s12613-018-1640-5.

[21] G. Golanski, J. Jasak, A. Zielinsky, C. Kolan, M. Urzynicok, P. Wieczorek, Quantitative analysis of stability of 9%Cr steel microstructure after long-term ageing, Arch. Metall. Mater. 62 (2017) 273–381, https://doi.org/10.1515/amm-2017-0040.

[22] R. Hernández, M. Serrano, A. García-Junceda, E. Oñorbe, J. Vivas, Improvement of High Temperature Creep Strength of Conventional Grade 91 Steel by Thermomechanical Treatments, Proc ASME. PVP2019, Volume 6B: Mater. Fabricat., V06BT06A012, https://doi.org/10.1115/PVP2019-93148.

[23] J. Vivas, C. Capdevila, J.A. Jimenez, M. Benito-Alfonso, D. San Martin, Effect of Ausforming Temperature on the Microstructure of G91 Steel, Metals 7 (7) (2017) 236, Doi: 10.3390/met7070236.

[24] S.S. Samant, I.V. Singh, R.N. Singh, Influence of intermediate rolling on mechanical behavior of modified)Cr-1Mo steel, Mat. Sci. Eng. A 738 (2018) 135–152, https://doi.org/10.1016/j.msea.2018.09.092.

[25] N. Roduit, JMicroVision, http://www.jmicrovision.com.

[26] P.M. Kelly, A. Jostsons, R.G. Blake, J.G. Napier, The determination of foil thickness by scanning transmission electron microscopy, Phys. Stat. Sol. (a) 31 (1975) 771–779, https://doi.org/10.1002/pssa.2210310251.

[27] D. Rojas, J. Garcia, O. Prat, G. Sauthoff, A.R. Kaysser-Pyzalla, 9%Cr heat resistant steels: Alloy design, microstructure evolution and creep response at 650 °C, Mater. Sci. Eng. A, 528 (2011) 5164-5176, Doi: 10.1016/j.msea.2011.03.037.

[28] J. Hald, L. Korcakova, Precipitate stability in creep resistant ferritic steels, Exp. Investigat. Model., ISIJ Int. 43 (2003) 420–427, https://doi.org/10.2355/isijinternational.43.420.

[29] Y. Du, X. Li, X.u. Zhang, Y.-W. Chung, D. Isheim, S. Vaynman, Design and Characterization of a Heat-Resistant Ferritic Steel Strengthened by MX Precipitates, Metall Mater Trans A 51 (2) (2020) 638–647.

[30] V. Thomas Paul, S. Saroja, M. Vijayalakshmi, Microstructural stability of modified 9Cr–1Mo steel during long term exposures at elevated temperatures, J. Nucl. Mater. 378 (3) (2008) 273–281.

[31] M. Li, W.-Y. Chen, Microstructure-based prediction of thermal aging strength reduction factors for grade 91 ferritic-martensitic steel, Mat. Sci. Eng. A 798 (2020), 140116, https://doi.org/10.1016/j.msea.2020.140116.

[32] T. Nakajima, S. Spigarelli, E. Evangelista, T. Endo, Strain enhanced growth of precipitates during creep of T91, Mater. Trans. 44 (9) (2003) 1802–1808, https://doi.org/10.2320/matertrans.44.1802.

[33] V. Samaee, R. Gatti, B. Devincre, T. Pardoen, D. Schryvers, H. Idrissi, Dislocation driven nanosample plasticity: new insights from quantitative in-situ tensile testing, Sci. Rep. 8 (2018) 12012, https://doi.org/10.1038/s41598-018-30639-8.

[34] L. Tan, Y. Yang, J.T. Busby, Effect of alloying elements and thermo-mechanical treatment on 9Cr Reduced Activation Ferritic-Martensitic (RAFM) steel, J. Nucl. Mater., 442 (2013) S13-S17, doi: 10.1016/j.jnucmat.2012.10.015.

[35] L. Chen, Z. Zeng, Y. Zhao, F. Zhu, X. Liu, Microstructures and High-Temperature Mechanical Properties of a Martensitic Heat-Resistant Stainless Steel 403Nb Processed by Thermo-Mechanical Treatment, Metall. Mater. Trans. A 45A (2014) 1498–1507, https://doi.org/10.1007/s11661-013-2105-0.

[36] C.X. Liu, Z.S. Yan, Z.Z. Dong, Y.C. Liu, B.Q. Ning, Effects of Two-Step Tempering Treatment on the Microstructural Formation of T91 Ferritic Steels, Solid State Phenom. 172–174 (2011) 875–880, https://doi.org/10.4028/www.scientific.net/ssp.172-174.875.

[37] Z. Shang, J. Ding, C. Fan, M. Song, J. Li, Q. Li, S. Xue, K.T. Hartwig, X. Zhang, Tailoring the strength and ductility of T91 steel by partial tempering treatment, Acta Mater. 169 (2019) 209–224, https://doi.org/10.1016/j.actamat.2019.02.043.

[38] R. Sarkar, C. Retenberger, J. Rajagopalan, Electron Beam Induced Artifacts during in situ TEM deformation of nanostructured metals, Scientific Reports 5 (2015) 16345, https://doi.org/10.1018/srep16345. doi: 10.1038/srep16345.